NANO · MICRO
small

Supporting Information

for *Small*, DOI 10.1002/smll.202406669

Sustainable Production of Biomass-Derived Graphite and Graphene Conductive Inks from Biochar

Haoyang You, Janan Hui, Yilun Zhou, Kayla Vittore, Jinrui Zhang, Lindsay E. Chaney, Sritarun Chinta, Yunhao Zhao, Gilhwan Lim, DoKyoung Lee, Elizabeth A. Ainsworth, Jennifer B. Dunn, Vinayak P. Dravid, Mark C. Hersam and Stuart J. Rowan**

Supporting Information

Sustainable Production of Biomass-Derived Graphite and Graphene Conductive Inks from Biochar

Haoyang You, Janan Hui, Yilun Zhou, Kayla Vittore, Jinrui Zhang, Lindsay E. Chaney, Sritarun Chinta, Yunhao Zhao, Gilhwan Lim, DoKyoung Lee, Elizabeth A. Ainsworth, Jennifer B. Dunn, Vinayak P. Dravid, Mark C. Hersam, Stuart J. Rowan**

Table of Contents

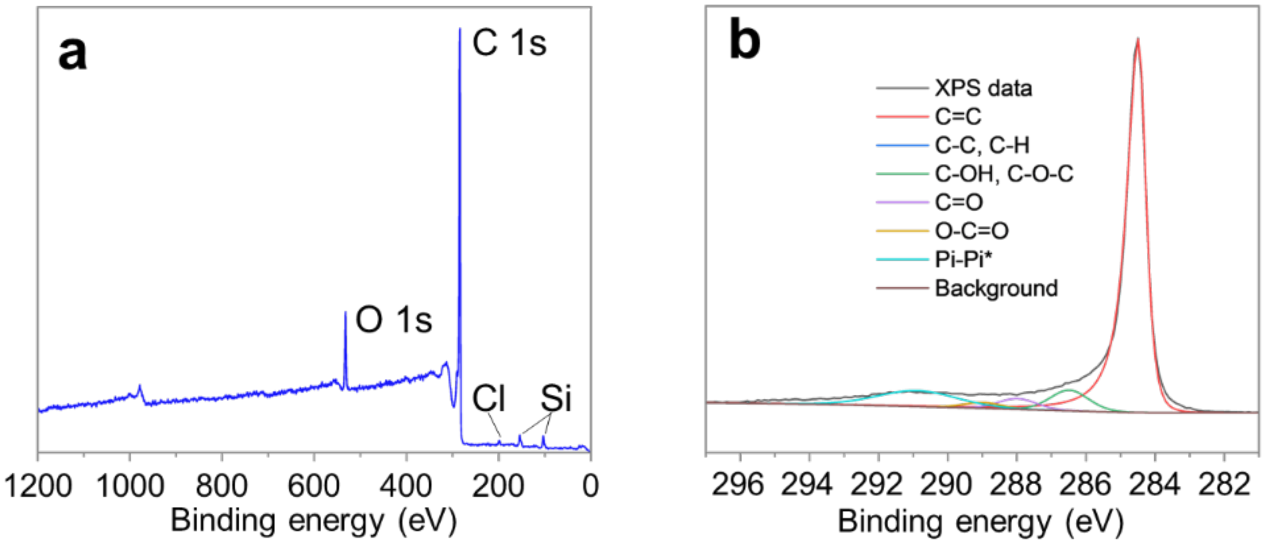

Figure S1. XPS spectra of hardwood derived bio-graphite. (a) XPS survey spectrum of bio-graphite, and (b) C 1s spectrum of XPS of bio-graphite and its peak fitting.

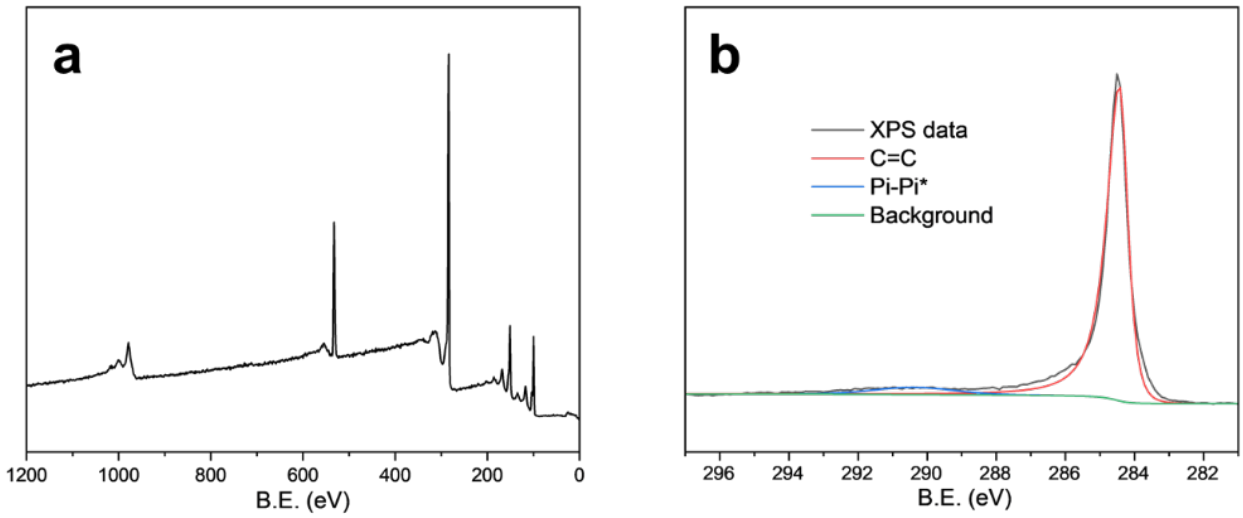

Figure S2. XPS spectra of natural graphite. (a) XPS survey spectrum of natural graphite; (b) C 1s spectrum of XPS of natural graphite and its peak fitting.

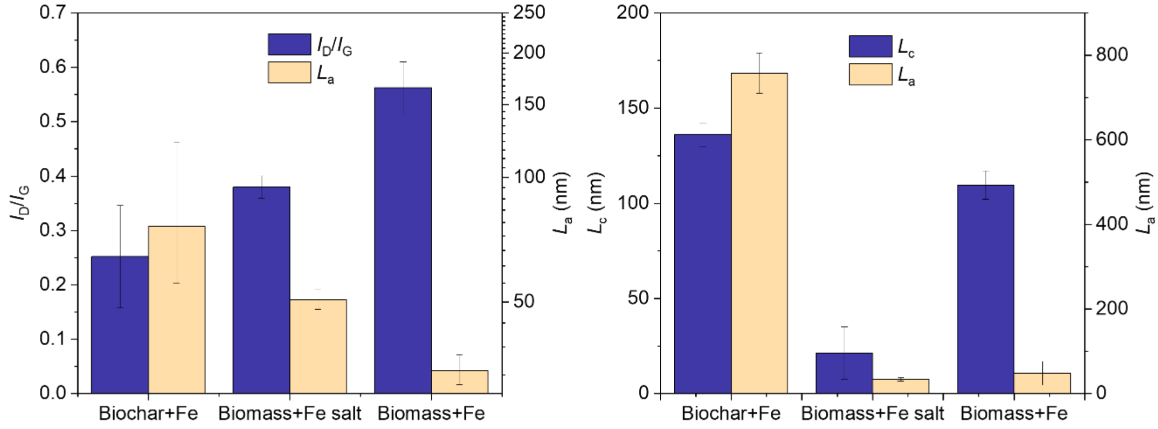

Figure S3. (a) I_D/I_G from Raman (n = 3, and data are presented as mean ± SD of all samples analyzed in each group) and corresponding graphite crystallite size in a-direction (L_a) of hardwood derived bio-graphite prepared with different methods, (b) graphite crystallite size in c-direction (L_c) and a-direction (L_a) of the hardwood derived bio-graphite prepared with different methods (n = 3, and data are presented as mean ± SD of all samples analyzed in each group).

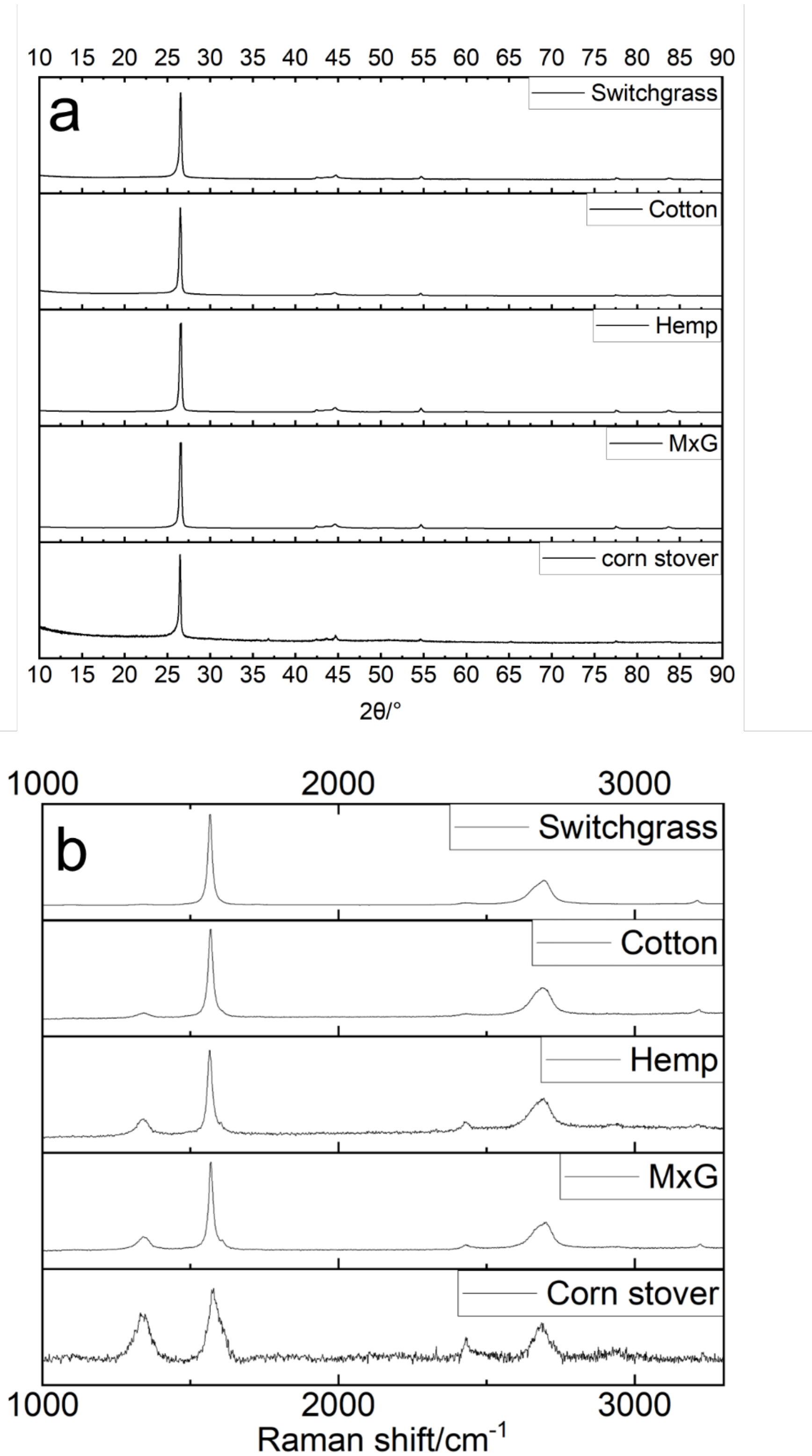

Figure S4. (a) XRD patterns and (b) Raman spectra of bio-graphite prepared with switchgrass, cotton, hemp, MxG, and corn stover.

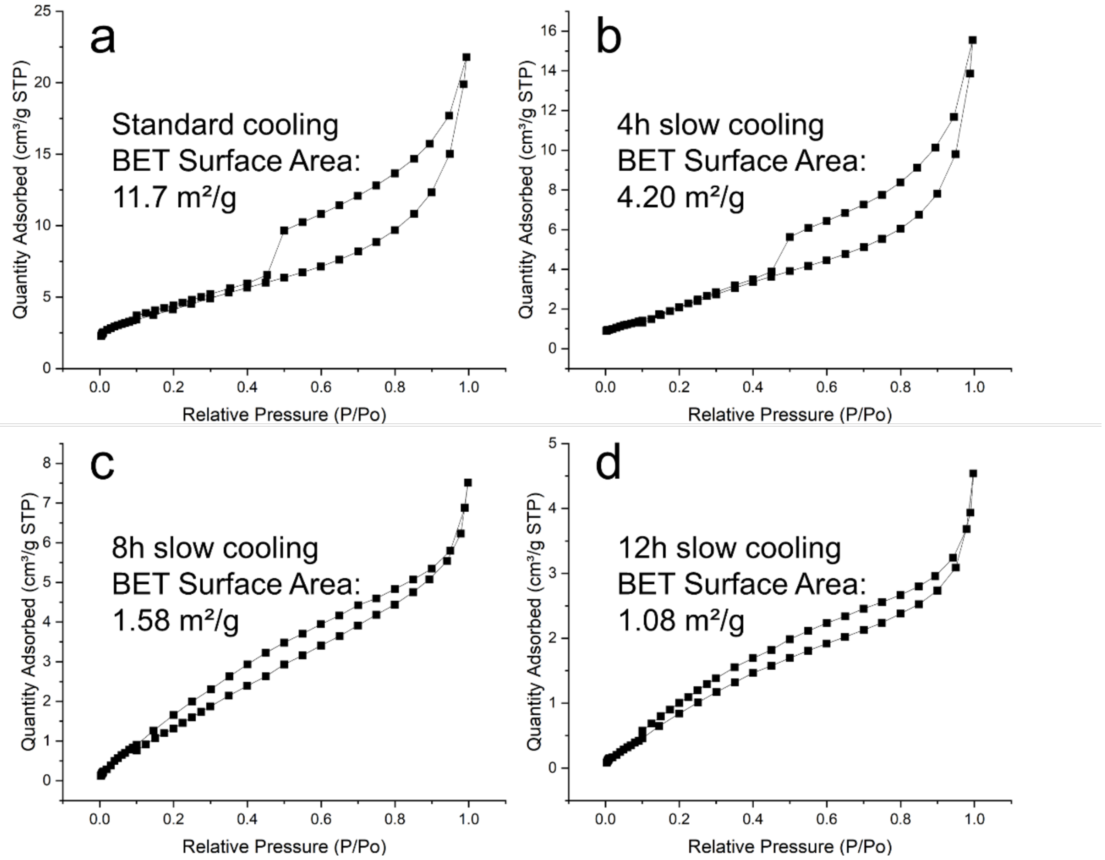

Figure S5. N_2 sorption isotherm for (a) standard cooling bio-graphite, (b) 4h slow cooling bio-graphite, (c) 8h slow cooling bio-graphite, and (d) 12h slow cooling bio-graphite.

Table S1. Life cycle inventory data per metric ton of product for our work and other bio-graphite synthesis methods.

	Our Work	Bio-graphite[1]	Bio-graphite[2]	Bio-graphite[3]	Bio-graphite[4]
Electricity (MJ)	14000	29000	16000	84000	27000
Sulfuric acid (kg) a)	240				
Iron (kg)a)	130	180			170
Biochar (kg)	1300				
Lignin (kg)			2800	5600	
Tetrahydrofuran (kg)			0.27		
Iron nitrate nonahydrate (kg) a)			900		
Hydrochloric acid (kg) a)		2700	2700		5400
Iron nitrate (kg) a)				120	
Manganese nitrate (kg)a)				310	
Cobalt nitrate (kg) a)				460	
Hardwood (kg)		5900			5400

a)All catalysts and acid are considered recoverable with an estimated 5% loss.

Table S2. Life cycle assessment results for different graphite synthesis methods. The environmental impact is reported as fossil fuel demands and green-house gas (GHG) emissions per metric ton of graphite produced.

	Fossil Fuels Demand (MJ)	GHG Emission (kg CO_2 eq)
Our Work	5.7×10^4	4.0×10^3
Natural graphite[5]	6.8×10^4	7.2×10^3
Synthetic graphite[5]	7.9×10^4	7.6×10^3
Bio-graphite[1]	1.2×10^5	9.0×10^3
Bio-graphite[2]	1.1×10^5	8.4×10^3
Bio-graphite[3]	1.7×10^5	1.4×10^4
Bio-graphite[4]	1.9×10^5	1.4×10^4

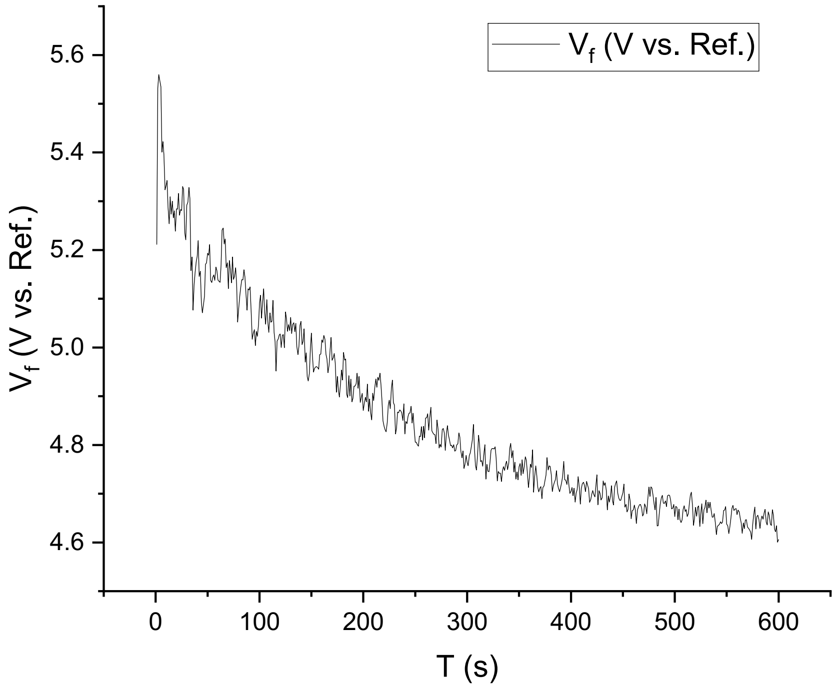

Figure S6. Recorded voltage plotted with time during the electroplating of acidic $FeSO_4$ solution at a constant current *I*=100 mA.

Table S3. Overview of production of printable graphene from biomass materials.

Biomass Source	Preheat Conditions	Pyrolysis conditions	Printing Type	Conductivity (S/m)	Ref
Lignin	275 °C, 30 min	1100 °C, 3 hr, $Ni(NO_3)_2$ cat.	Rod-coating	47	[6]
Microfibrillated cellulose	110 °C, 48 hr	800 °C, 30 min	3D-print	55	[7]
Hemp Bast fiber	180 °C, 24 hr	800 °C, 1 hr, KOH	Pressed Composite	226	[8]
Walnut Shells	500 °C, 1 hr	800 °C, 3 hr, KOH	Pressed composite	720	[9]
Silkworm Shell	-	1000 °C, 2 hr, $FeCl_3$ cat.	Vacuum-filter	760	[10]
Glucose	600 °C, 2 hr	800 °C, 6 hr	Pressed composite	785	[11]
Peanut seed Coats	-	1000 °C, 2 hr, triethanolamine	Pressed composite	810	[12]
Filter Paper	250 °C, 8 hr	1000 °C, 3 hr, Fe_3O_4, GO	Pressed paper	1500	[13]
Hardwood	-	30W Laser	Screen-print	2800	[14]
Cellulose acetate	Dried 4 hr	800 °C, 2 hr, Graphene Oxide	Pressed composite	4900	[15]
Coconut Shells	400 °C, 3 hr	900 °C, 2 hr, K_2CO_3	Pressed composite	3214	[16]
Sawdust	450 °C, 2 hr	1000 °C, 3 hr, $FeCl_3$ cat.	Vacuum-filter, compress	3670 (Vacc) 13900 (pellet)	[17]
Wood	350 °C, 1 hr	1500 °C, 1 hr	Pressed composite	8500 (pellet)	[18]
Microcrystalline cellulose	100 °C/h to 250 °C, 3 h dwell; 5 °C/h to 275 °C, 2 h dwell; 5 °C/h to 325 °C, 2 h dwell; 50 °C/h to 450 °C, 1 h dwell	1200-2000 °C, 12 hr	Pressed composite	10000	[19]
This Work	1100 °C, 1 hr	1200 °C, 1 hr (4 hr Slow cool)	Spin-coat, Screen print	23530 (Screen-print) 35750 (Spin)	-

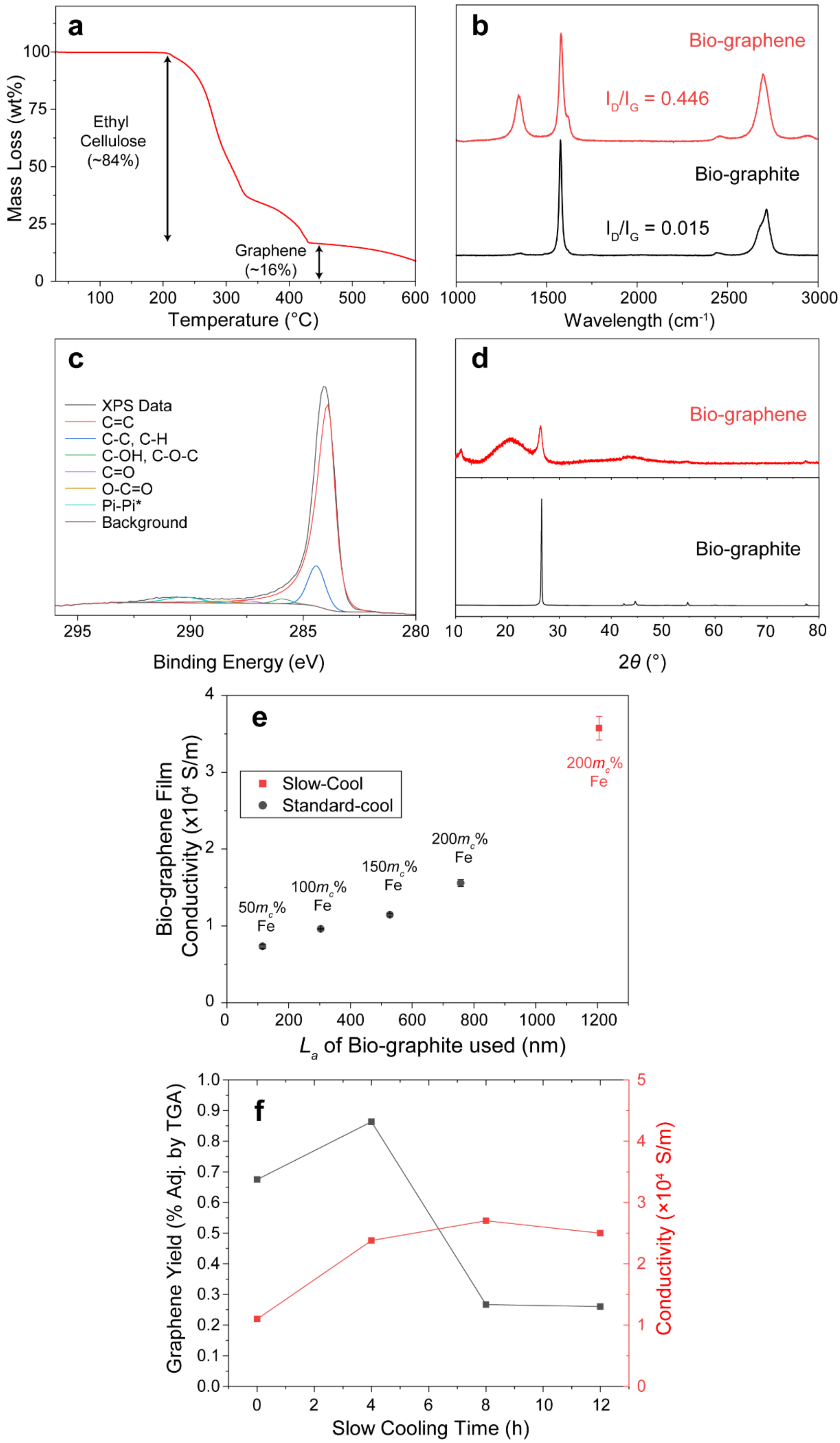

Figure S7. (a) Thermogravimetric analysis of Biographene/Ethyl Cellulose powder composite, (b) Raman spectra of slow cooling hardwood bio-graphite and exfoliated bio-graphene. (c) C1s region of XPS for the exfoliated bio-graphene. (d) XRD profiles of slow cooling hardwood bio-graphite and exfoliated bio-graphene. (e) Relationship of L_a of bio-graphite as modulated by the iron catalyst content and the conductivity of spin-coated films from the exfoliated bio-graphene material (n = 3, and data are presented as mean ± SD of all samples analyzed in each group), and (f) Effect of slow cooling time on the graphene yield (adjusted by the pure graphene product based on TGA at 350°C), and graphene conductivity of spin-coated films.

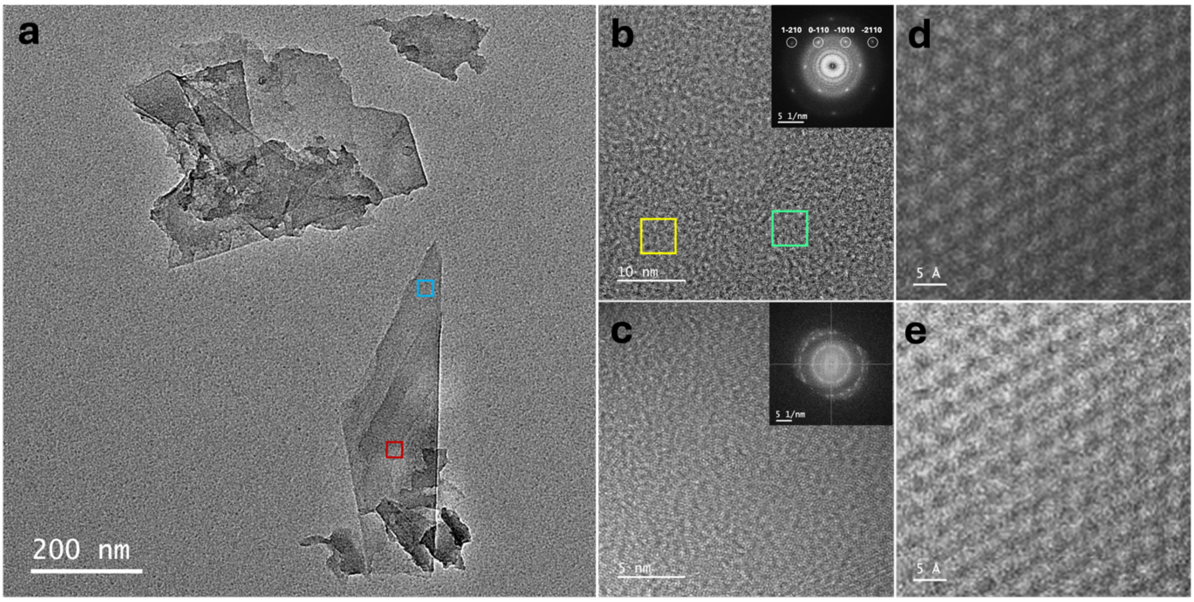

Figure S8. HRTEM characterization of monolayer and few-layer bio-graphite exfoliated bio-graphene flakes. (a) TEM image of graphene flakes, consisting of various layers of graphene. (b) HRTEM image of the blue-squared region in (a), representative of monolayer graphene. The inset is an FFT of the image, displaying the typical sixfold symmetry. The inner peaks have higher intensity than the outer ones, confirming that this region is indeed a monolayer. (c) HRTEM image of the red-squared region in (a), representative of few-layer graphene. Visually it is clear that different lattice planes are oriented in multiple geometries throughout the field-of-view. The inset is an FFT of the image, showing multiple staggered hexagonal stacking behavior, confirming many graphene layers stacked on top of one another in various orientations. (d-e) Atomic-resolution HRTEM images of the green-squared and yellowsquared regions in (b), respectively, showing the clear hexagonal in-plane lattice structure of graphene.

References

[1] W. J. Sagues, J. Yang, N. Monroe, S.-D. Han, T. Vinzant, M. Yung, H. Jameel, M. Nimlos, S. Park, *Green Chem.* **2020**, *22*, 7093.

[2] Q. Yan, X. Zhang, J. Li, E. B. Hassan, C. Wang, J. Zhang, Z. Cai, *J. Mater. Sci.* **2018**, *53*, 8020.

[3] M. Demir, Z. Kahveci, B. Aksoy, N. K. R. Palapati, A. Subramanian, H. T. Cullinan, H. M. El-Kaderi, C. T. Harris, R. B. Gupta, *Ind. Eng. Chem. Res.* **2015**, *54*, 10731.

[4] N. A. Banek, D. T. Abele, K. R. McKenzie, M. J. Wagner, *ACS Sustain. Chem. Eng.* **2018**, *6*, 13199.

[5] Argonne National Laboratory, The Greenhouse Gases, Regulated Emissions, and Energy Use in Technologies (GREET) Model, https://www.energy.gov/eere/greet, accessed: Jan., **2022**.

[6] B. N. Altay, B. Aksoy, D. Banerjee, D. Maddipatla, P. D. Fleming, M. Bolduc, S. G. Cloutier, M. Z. Atashbar, R. B. Gupta, M. Demir, *ACS Appl. Electron. Mater.* **2021**, *3*, 3904.

[7] Y. Shao, D. Chaussy, P. Grosseau, D. Beneventi, *Ind. Eng. Chem. Res.* **2015**, *54*, 10575.

[8] H. Wang, Z. Xu, A. Kohandehghan, Z. Li, K. Cui, X. Tan, T. J. Stephenson, C. K. King'ondu, C. M. B. Holt, B. C. Olsen, J. K. Tak, D. Harfield, A. O. Anyia, D. Mitlin, *ACS Nano* **2013**, *7*, 5131.

[9] T. Shang, Y. Xu, P. Li, J. Han, Z. Wu, Y. Tao, Q.-H. Yang, *Nano Energy* **2020**, *70*, 104531.

[10] W. Tian, Q. Gao, A. VahidMohammadi, J. Dang, Z. Li, X. Liang, M. M. Hamedi, L. Zhang, *Chem. Eng. J.* **2021**, *420*, 127601.

[11] X. Li, S. Kurasch, U. Kaiser, M. Antonietti, *Angew. Chem. Int. Ed.* **2012**, *51*, 9689.

[12] B. Liu, M. Yang, D. Yang, H. Chen, H. Li, *J. Power Sources* **2020**, *456*, 227999.

[13] T. Gao, C. Xu, R. Li, R. Zhang, B. Wang, X. Jiang, M. Hu, Y. Bando, D. Kong, P. Dai, X.-B. Wang, *ACS Nano* **2019**, *13*, 11901.

[14] J. Edberg, R. Brooke, O. Hosseinaei, A. Fall, K. Wijeratne, M. Sandberg, *npj Flex. Electron.* **2020**, *4*, 17.

[15] V. Kuzmenko, N. Wang, M. Haque, O. Naboka, M. Flygare, K. Svensson, P. Gatenholm, J. Liu, P. Enoksson, *RSC Adv.* **2017**, *7*, 45968.

[16] J. Xia, N. Zhang, S. Chong, D. Li, Y. Chen, C. Sun, *Green Chem.* **2018**, *20*, 694.

[17] S.-J. Yuan, B. Dong, X.-H. Dai, *Appl. Surf. Sci.* **2021**, *562*, 150203.

[18] Y.-J. Liou, W.-J. Huang, in *Electroplating of Nanostructures*, InTech, **2015**.

[19] Y.-R. Rhim, D. Zhang, D. H. Fairbrother, K. A. Wepasnick, K. J. Livi, R. J. Bodnar, D. C. Nagle, *Carbon* **2010**, *48*, 1012.